

The mouse stargazer gene encodes a neuronal Ca²⁺-channel γ subunit

Verity A. Letts¹, Ricardo Felix², Gloria H. Biddlecome², Jyothi Arikath², Connie L. Mahaffey¹, Alicia Valenzuela¹, Frederick S. Bartlett II¹, Yasuo Mori³, Kevin P. Campbell² & Wayne N. Frankel¹

Stargazer mice have spike-wave seizures characteristic of absence epilepsy, with accompanying defects in the cerebellum and inner ear. We describe here a novel gene, *Cacng2*, whose expression is disrupted in two stargazer alleles. It encodes a 36-kD protein (stargazin) with structural similarity to the γ subunit of skeletal muscle voltage-gated calcium (Ca²⁺) channels. Stargazin is brain-specific and, like other neuronal Ca²⁺-channel subunits, is enriched in synaptic plasma membranes. *In vitro*, stargazin increases steady-state inactivation of α_1 class A Ca²⁺ channels. The anticipated effect in stargazer mutants, inappropriate Ca²⁺ entry, may contribute to their more pronounced seizure phenotype compared with other mouse absence models with Ca²⁺-channel defects. The discovery that the stargazer gene encodes a γ subunit completes the identification of the major subunit types for neuronal Ca²⁺ channels, namely α_1 , $\alpha_2\delta$, β and γ , providing a new opportunity to understand how these channels function in the mammalian brain and how they may be targeted in the treatment of neuroexcitability disorders.

Introduction

Epilepsies are a heterogeneous group of disorders characterized by recurrent spontaneous seizures affecting 1% of the population. Approximately half of epilepsy cases are thought to have some genetic component, but the heterogeneity and complexity of the genes makes them difficult to map¹. Relatively few epilepsies can be explained by a single gene mutation, but in recent years several human genes have been identified, including most recently those encoding the potassium channels KCNQ2 and KCNQ3, whose mutations cause benign familial neonatal convulsions²⁻⁴.

A number of mouse mutants have generalized tonic-clonic seizures, mostly resulting from gene knockouts. Ion channels are involved in many of these cases, including potassium⁵, GABA (ref. 6) and glutamate receptor channels⁷. Comparatively fewer mouse models have been described with absence seizures, (also known as petit-mal or spike-wave), although this may be due to ascertainment bias, as these seizures are associated with only a brief loss of consciousness. It has thus required a systematic electrocorticographic screen of known mutants to uncover mouse absence models⁸. The mouse mutants ducky, lethargic, mocha, slow-wave epilepsy, stargazer and tottering each show some form of spike-wave discharge associated with behavioural arrest, which is characteristic of absence epilepsy⁸⁻¹⁰. The underlying genes are described in most of these models, and in two—tottering and lethargic—the defect is in a gene encoding a neuronal Ca²⁺-channel subunit^{11,12}.

Voltage-gated Ca²⁺ channels are a diverse family of proteins that have a variety of biological functions, including presynaptic neurotransmitter release and protein signalling within the cell^{13,14}. The Ca²⁺ currents produced by these channels are classified into P/Q-, N-, L-, R- and T-type based on their pharmacological and biophysical properties, and all are expressed in brain¹⁵⁻¹⁷. Except for T-type, whose molecular structure is unknown, all voltage-gated Ca²⁺ channels are composed of at least three sub-

units, α_1 , $\alpha_2\delta$ and β (ref. 18). A fourth subunit, γ , is associated with skeletal muscle Ca²⁺ channels. The mRNA for this γ subunit is abundant in skeletal muscle, but has not been detected in brain^{19,20}. The α_1 subunit forms the membrane pore and voltage-sensor and is a major determinant for current classification. The other subunits modulate the voltage-dependence and kinetics of activation and inactivation, and the current amplitude²¹. P/Q- and N-type channels purified from brain contain α_{1A} and α_{1B} subunits, respectively. These α_1 subunits are associated with various proportions of four separately encoded β subunit proteins, indicating that considerable subunit complexity exists, even for channels that produce only one type of current^{22,23}.

Because of the overlap in expression of voltage-gated Ca²⁺-channel subunits and current subtypes in brain, study of channel subunit function *in vivo* has not been straightforward. The study of mouse mutations has begun to allow a dissection of this problem. For example, the neurological mutants tottering and lethargic have defects in genes encoding α_{1A} and β_4 subunits, respectively^{11,12}. Their phenotypes are very similar, each showing spike-wave seizures and moderate cerebellar ataxia without obvious neuronal damage. The mutation in each is commensurate with the respective roles of major and auxiliary Ca²⁺-channel subunits: tottering has an amino acid substitution in the structural α_{1A} subunit, whereas lethargic is not likely to express any functional β_4 protein. The phenotype of the lethargic mouse shows that defects in regulatory subunits can also lead to the same neuronal malfunctions observed for structural subunit mutations. Continued study of these mouse mutants should give further insight into neuronal Ca²⁺-channel function *in vivo*, although a comprehensive understanding requires the identification of all the major subunits.

The stargazer mutation arose spontaneously at The Jackson Laboratory on the A/J inbred mouse line⁹, and was initially detected for its distinctive head-tossing and ataxic gait. Subsequent

¹The Jackson Laboratory, Bar Harbor, Maine 04609, USA. ²Howard Hughes Medical Institute, Department of Physiology and Biophysics and Department of Neurology, The University of Iowa College of Medicine, Iowa City, Iowa 52242, USA. ³Department of Information Physiology, National Institute for Physiological Sciences, Okazaki, Japan. Correspondence should be addressed to W.N.F. (e-mail: wnf@jax.org) or V.A.L. (e-mail: val@jax.org).

electrocorticography revealed recurrent spike-wave seizures when the animal was still, characteristic of absence epilepsy. The seizures were notably more prolonged and frequent than in tottering or lethargic mice, lasting on average six seconds and recurring over one-hundred times per hour. The ataxia and head-tossing are presumed to be pleiotropic consequences of the mutation in the cerebellum and inner ear, respectively; the latter also distinguishes stargazer from the other mutants. The waggler mutant arose independently on the MRL/MpJ strain; its genetic defect was subsequently found to be allelic to that of stargazer²⁴. Waggler mice are severely ataxic, but head-toss less frequently than stargazer and have a more pronounced side-to-side head motion.

In an earlier study, we described the fine-mapping of the stargazer mutation on mouse chromosome 15 and the construction of a 1.3-Mb physical contig across the critical genetic interval²⁵. Here we describe a new gene disrupted in stargazer and waggler mice. The structural and functional similarity of stargazer to the γ subunit of skeletal muscle voltage-gated Ca^{2+} channels suggests that it encodes the first described neuronal Ca^{2+} -channel γ subunit. Its defect in stargazer mice shows that this new gene is critical for normal function of the central nervous system.

Results

An ETn insertion mutation in the stargazer critical interval

Our previously described 1.3-Mb contig of DNA critical to the stargazer phenotype was comprised of YAC, P1 and BAC recombinant DNA clones. To identify candidate genes we performed direct cDNA selection²⁶ on the two clones, P12 and BAC28, which spanned the stargazer critical interval as defined by genetic recombination²⁵. Selection products were screened for expression or structural defects in stargazer mice. Using Southern-blot hybridization of genomic DNA from mutants and controls, clone c144 identified a 9-kb *Hind*III fragment in stargazer homozygotes, but a 12-kb fragment (BG11) in wild-type A/J mice, the strain on which the stargazer mutation arose (data not shown). Comparative sequencing showed that six further cDNA selection products were from BG11 (Fig. 1a), including c416. On Southern blots, clone c416 identified a 9-kb *Bam*HI fragment from

stargazer, compared with a 3-kb *Bam*HI fragment derived from the A/J strain (data not shown). The hybridization results were consistent with an approximately 6-kb DNA insertion, containing no *Bam*HI sites but at least one asymmetrically positioned *Hind*III site (Fig. 1a). Although several different types of spontaneous proviral insertion mutations have been described in mice, the putative size and restriction map at stargazer was consistent with that of an early transposon (ETn). To test this hypothesis, PCR and sequencing was carried out using oligonucleotides based on the ETn long terminal repeats (LTR), and flanking genomic DNA from A/J and stargazer mutants, including both homozygous and heterozygous genotypes from the B6C3Fe-*stg* stock and the intersubspecific mapping cross²⁵ (Fig. 1b). Discrete PCR-generated fragments between the LTR primers and the flanking DNA were observed in stargazer mutants (Fig. 1b, s/s) or heterozygotes (+/s), but not in wild-type controls (+/+), showing that an ETn insertion was only associated with the stargazer mutation.

A novel gene resides at the stargazer locus

Of the cDNA selection products mapping to BG11, only c113 contained a long open reading frame (ORF), 83 bp of which was present in BG11 as a putative exon (Fig. 1a). To explore the coding potential of c113, a mouse brain cDNA library was screened and three clones were sequenced. The longest clone, c2, was over 2.5 kb and included an ORF of 969 bp encoding a putative protein of 323 aa, or 36 kD (Fig. 2a). DNA hybridizations and BAC sequencing confirmed that much of c2 originated from BAC28. However, sequences corresponding to more 5' exons, including the first 70 aa of the putative coding region, were not found on BAC 28, but were located on two P1 clones from a more telomeric portion of the contig (Fig. 1a). The corresponding 4.5-kb *Hind*III fragment containing this sequence (including exon 1 and the putative 5' untranslated region) was partly sequenced, confirming that the 5' portion of c2 comes from this region. These results are consistent with the stargazer gene having four exons, with intron 1 of 50–90 kb spanning at least two recombinants from the intersubspecific cross. The ETn insertion resides in intron 2 in the same transcriptional orientation as the stargazer gene.

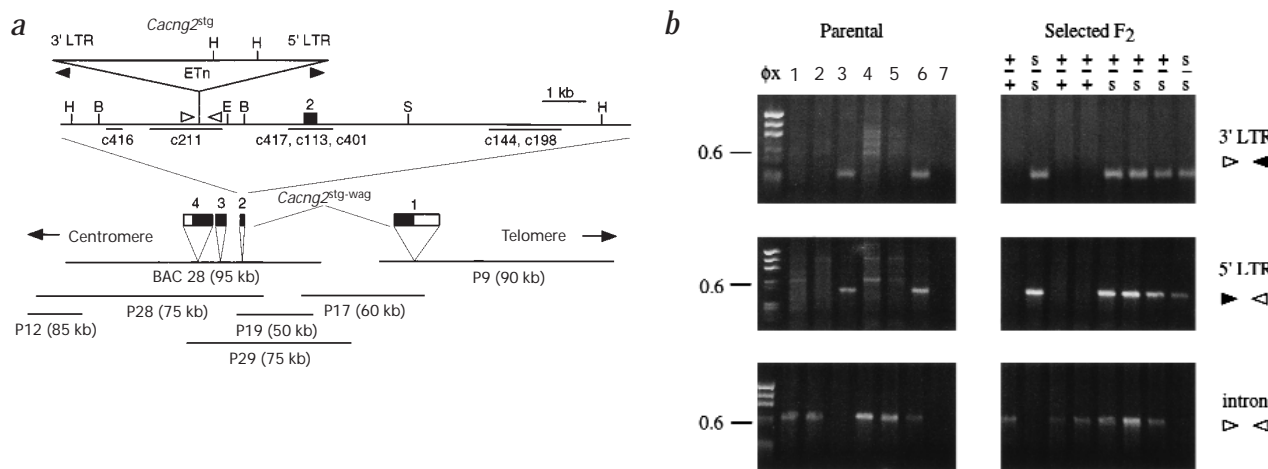


Fig. 1 An ETn insertion is genetically and physically linked with the *stg* locus on mouse chromosome 15. **a**, Restriction map of the 12-kb *Hind*III fragment from BAC28, showing the locations of exon 2, cDNA selection products 416, 211, 417, 113, 401, 144, 198 and the ETn insertion. B, *Bam*HI; E, *Eco*RI; H, *Hind*III; S, *Sac*I. Several additional *Bam*HI sites are not shown. The locations of oligonucleotide primers used (Fig. 1b) are shown here as filled arrowheads (left, ETn-OR; right, JS167) and open arrowheads (left, 109F; right, E/Ht7). Below the restriction map are the exons from cDNA clone c2 shown relative to the mouse BAC and P1 contig²⁵. Coding regions are shown in black, untranslated regions in white. Splice site sequences will be provided upon request. **b**, Genomic DNA PCR reactions generated by primers (Fig. 1a, arrowheads) spanning the 5' LTR-intron junction (oligonucleotides JS167 and E/Ht7), the 3' LTR-intron junction (ETn-OR and 109F) or intron flanking primers (109F and E/Ht7) spanning the wild-type allele of the ETn integration site. The frames on the left are parental strain, hybrid DNA and control including lanes: 1, C57BL/6J; 2, A/J; 3, B6C3Fe-*stg/stg*; 4, MRL/MpJ; 5, B6 - *stg^{wag}/stg^{wag}*; 6, (B6C3-*stg* x B6 - *stg^{wag}*)-F₁ hybrid (compound heterozygote); and 7, no genomic DNA (water control). The frames on the right are selected recombinants of known *stg* genotype from the intersubspecific F₂ stargazer cross DNA (ref. 25), including wild-type (+/+), +*stg* (+/s) and *stg/stg* (s/s) genotypes. The size marker is *Hae*III restriction-digested PhiX DNA (ϕ x).

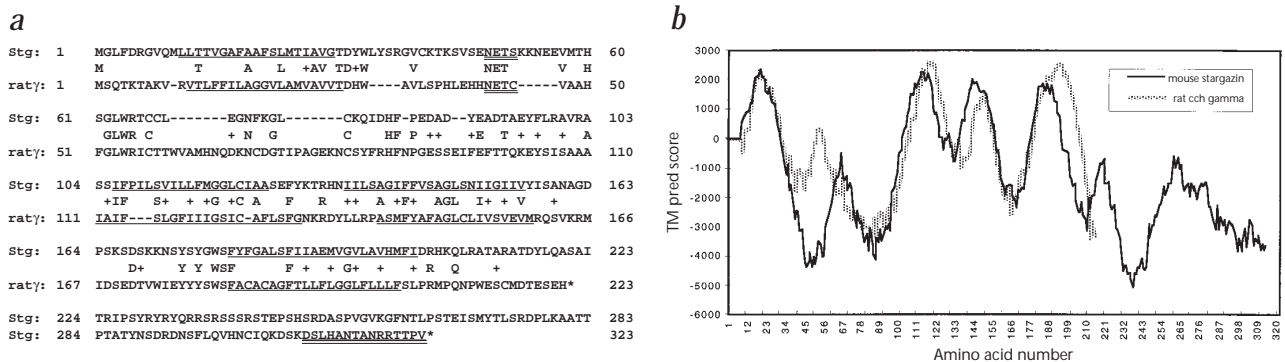


Fig. 2 Stargazin protein sequence and similarity to the γ subunit of voltage-gated skeletal muscle Ca^{2+} channels. **a**, The predicted open reading frame of cDNA clone c2 is shown on the top line (323 aa) and is aligned with that of the rat Ca^{2+} -channel γ subunit (223 aa) on the bottom line. The pairwise protein sequence alignment corresponding to stargazin aa 23–207 was made using Gapped BLAST (ref. 58), and the remaining residues were aligned manually. Alignments with human, rabbit and mouse Ca^{2+} -channel γ subunits are very similar (data not shown). Underlined sequences in each are putative transmembrane regions predicted by the program TM Pred (ref. 59). The predicted N-glycosylation sites are shown in double underline, and triple underline at the C terminus indicates the peptide used for antibody (Fig. 5). **b**, Secondary structure prediction plot made using TM Pred (ref. 59). Positive scores show residues that are likely to be in the membrane, and negative scores show those that are not.

The intron/exon junctions for the mouse stargazer gene were determined from our sequencing of the mouse cDNA, P1 and BAC (Fig. 1, legend). The sequences match consensus splice sites, except for the exon 2 splice donor sequence with a TCC/GT motif, confirmed in multiple independent cDNA and genomic DNA clones. This four exon configuration, with a very large first intron, is consistent with a partial sequence from the putative human stargazer homologue produced by the chromosome 22 sequencing group at the Sanger Centre; PAC dJ293L6 contains exon 1 and DNA at least 70 kb more centromeric, exons 3 and 4 are present on neighbouring PAC dJ1119A7. The putative translations of human exons 1, 3 and 4 show 98% identity with the corresponding mouse sequence. Presently, no epilepsy genes have been mapped to human chromosome 22q12–13, but as most epilepsy genes remain unmapped, this will be an important locus to check for novel linkages in the future.

Secondary-structure analysis suggests that the stargazer gene encodes a membrane-spanning protein (stargazin), with a

cytosolic amino terminus, four transmembrane domains and a cytosolic carboxy terminus. Although the protein is not highly similar to any previously described, it shares a modest partial sequence similarity (25% identity, 38% similarity over 200 aa; Fig. 2a), and predicted secondary structure (Fig. 2b) with the γ subunit of the skeletal muscle voltage-gated Ca^{2+} channel^{19,27,28}, a protein that spans the membrane four times and is shorter than stargazin by 100 aa at the C terminus. In addition, the exon structure is similar between the two genes²⁸.

Cacng2 mRNA expression

Blot hybridizations of adult total RNA from parental mouse strains using the c2 DNA as a probe revealed a brain-specific RNA of approximately 6–7 kb, a smaller, less abundant band of 3 kb and several minor species (Fig. 3a). The smaller transcript was consistent with the c2 cDNA clone, and blot analyses using BAC28-derived probes several kilobases downstream of the 3'

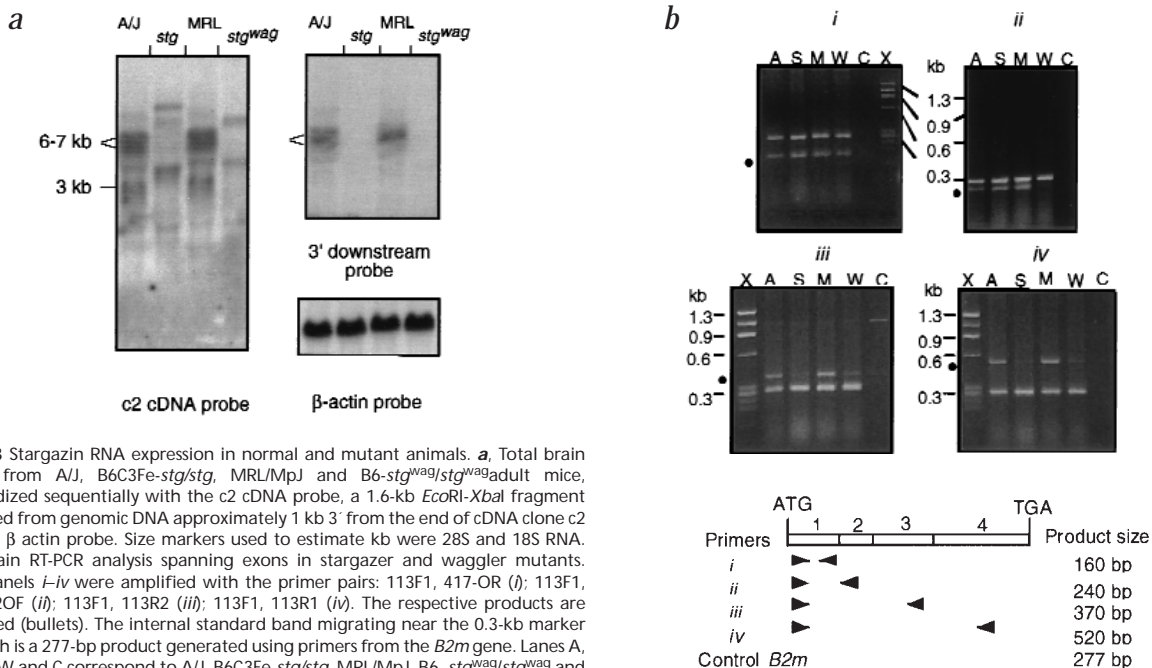
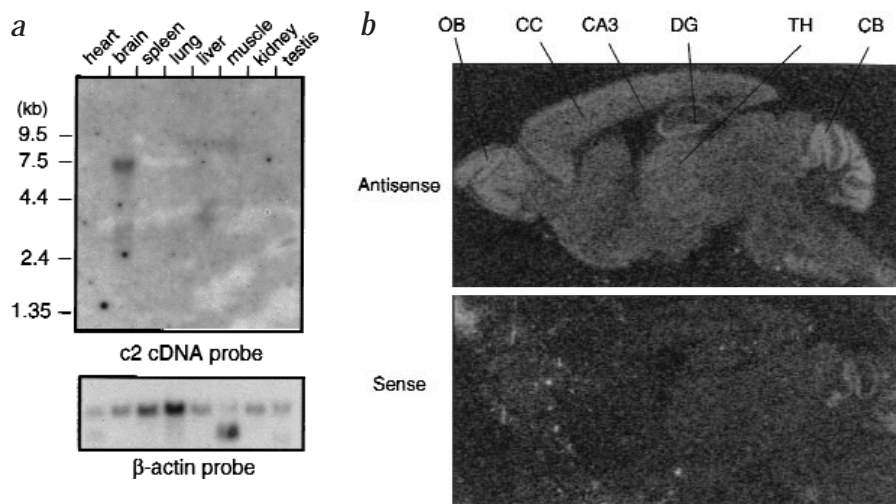


Fig. 3 Stargazin RNA expression in normal and mutant animals. **a**, Total brain RNA from A/J, B6C3Fe-*stg/stg*, MRL/MpJ and B6-*stg^{wag}/stg^{wag}* adult mice, hybridized sequentially with the c2 cDNA probe, a 1.6-kb *EcoRI-XbaI* fragment derived from genomic DNA approximately 1 kb 3' from the end of cDNA clone c2 and a β actin probe. Size markers used to estimate kb were 28S and 18S RNA. **b**, Brain RT-PCR analysis spanning exons in stargazer and waggler mutants. Subpanels i–iv were amplified with the primer pairs: 113F1, 417-OR (i); 113F1, Exon2OF (ii); 113F1, 113R2 (iii); 113F1, 113R1 (iv). The respective products are marked (bullets). The internal standard band migrating near the 0.3-kb marker in each is a 277-bp product generated using primers from the *B2m* gene. Lanes A, S, M, W and C correspond to A/J, B6C3Fe-*stg/stg*, MRL/MpJ, B6-*stg^{wag}/stg^{wag}* and no DNA (water) control, respectively, and lane X is the size marker (*HaeIII* restriction-digested ϕ X DNA).

Fig. 4 Stargazin RNA distribution. **a**, Northern blot purchased from a commercial source (Clontech) containing poly A⁺ RNA from multiple adult mouse tissues hybridized sequentially to the c2 cDNA probe and then the β actin probe, as shown. Size markers are from a RNA ladder provided on the blot by Clontech. **b**, RNA *in situ* hybridization using radiolabelled antisense and sense strand cRNA probes hybridized to paraformaldehyde-fixed sagittal sections from adult C57BL/6J mice. Some non-specific labelling is present in sense but is lower than in antisense. Regions of high specific expression include the cerebral cortex (CC), cerebellum (CB), hippocampal CA3 region (CA3), dentate gyrus (DG), olfactory bulb (OB), and thalamus (TH). The results shown are representative of several independent sections in separate experiments.



end of c2 showed specific hybridization to this larger 6–7-kb species, suggesting that these messages contained long 3' untranslated regions. Both major species were absent from stargazer and waggler mutant mice, and were replaced by less abundant, larger species (Fig. 3a). However, semi-quantitative RT-PCR using oligonucleotide primers from several different regions of the stargazin mRNA showed that both stargazer and waggler mutants produced at least some normally spliced mRNA (Fig. 3b); therefore, neither represents a completely null mutation. The stargazin transcript level is appreciably lower than wild-type downstream of exon 2, suggesting that the ETn insertion causes either premature transcriptional termination or inefficient splicing. Similarly, in the waggler allele, transcripts containing exon 1 are detectable at control levels, but those from downstream exons 2, 3 and 4 were much less abundant. Thus, although the waggler mutation is not yet known, by analogy with stargazer it appears to reside in intron 1.

Stargazin mRNA was expressed in adult mouse brain but not in heart, spleen, lung, liver, skeletal muscle, kidney or testis, as determined by RT-PCR (data not shown) and northern blots (Fig. 4a). RT-PCR of total RNA derived from cortex, midbrain, hippocampus, pons, cerebellum and olfactory bulb suggested that the protein is ubiquitously expressed in the brain (data not shown). RNA *in situ* hybridization confirmed this, showing highest expression in cerebellum, olfactory bulb, cerebral cortex, thalamus and CA3 and dentate gyrus regions of the hippocampus (Fig. 4b).

Stargazin localizes to synaptic membranes

To analyse the stargazin protein in native tissue, we developed a polyclonal antibody against the last 15 amino acids by injection of a KLH-coupled peptide into rabbits. Antibody 239 recognizes MBP-stargazin fusion protein, *in vitro* translated protein and

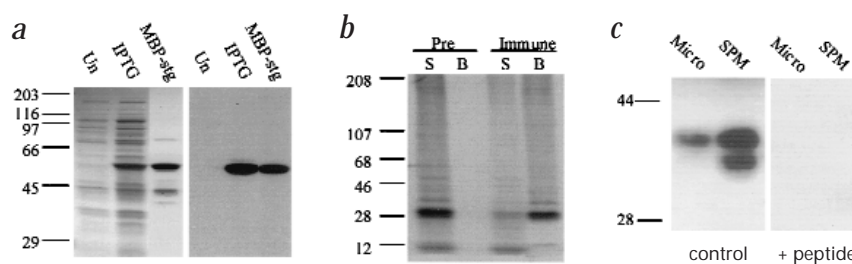
native stargazin in brain (Fig. 5). Its specificity for stargazin is shown by its detection of only the MBP-stargazin fusion protein in crude *E. coli* cell lysates (Fig. 5a). In addition, excess BSA-coupled antigenic peptide (Fig. 5c) and MBP-stargazin fusion protein (data not shown) completely inhibited binding of antibody 239 to stargazin in brain and synaptic plasma membrane preparations. Finally, stargazin antibody, but not preimmune serum, recognized and immunoprecipitated the stargazin *in vitro* translation product (Fig. 5b). This result also verifies that cDNA derived from the c2 clone contains a recognized ORF that is translated into protein.

As expected from the mRNA expression pattern (Fig. 4), stargazin is present in mouse brain, where the antibody recognized a 38-kD protein (Fig. 5c). This band is enriched in mouse synaptic plasma membranes, similar to neuronal Ca²⁺-channel subunits²⁹. As preliminary studies indicate that stargazin is glycosylated (data not shown), a size of 38-kD is consistent with the predicted translation and a N-glycosylation moiety (Fig. 2a). Synaptic plasma membranes also contain a 35-kD protein not seen in microsomes, even after long ECL exposures; this may represent an unglycosylated form. Future studies will clarify the structure and identity of these proteins.

Stargazin affects Ca²⁺-channel kinetics *in vitro*

Previous studies employing recombinant dihydropyridine (DHP)-sensitive voltage-dependent cardiac L-type Ca²⁺ channels showed that the γ subunit has a pronounced effect on the macroscopic characteristics of the currents transiently expressed in *Xenopus laevis* oocytes^{30,31} or in the mammalian HEK293 cell line^{27,32}. Given the structural similarities between stargazin and the skeletal muscle γ subunit, we investigated whether stargazin could modify the biophysical properties of neuronal voltage-

Fig. 5 Western-blot analysis and immunoprecipitation of stargazin. **a**, Cell lysates from *E. coli* transformed with pMal-*stg* before (Un) and after induction (IPTG; 100 cell equivalents each) and purified MBP-stargazin fusion protein (MBP-*stg*) were separated on a 10% SDS polyacrylamide gel. Gels were either stained with Gelcode (CB) or immunoblotted with affinity-purified antibody 239. **b**, The stargazer gene was transcribed and translated *in vitro* in the presence of [³⁵S]-Met, then immunoprecipitated with crude antibody 239 serum (Immune) or preimmune serum (Pre). One-third of the supernatant (S) and all of the bead elution (B) was loaded on a 5–16% SDS-polyacrylamide gel. **c**, Mouse KCl-washed brain microsomes (Micro) and synaptic plasma membranes (SPM; 200 μ g each) were electrophoresed on a 10% SDS-polyacrylamide gel and western-blot analysis was done with affinity-purified antibody 239 in the absence (control) or presence (+ peptide) of 50 μ g/ml BSA-coupled antigenic peptide.



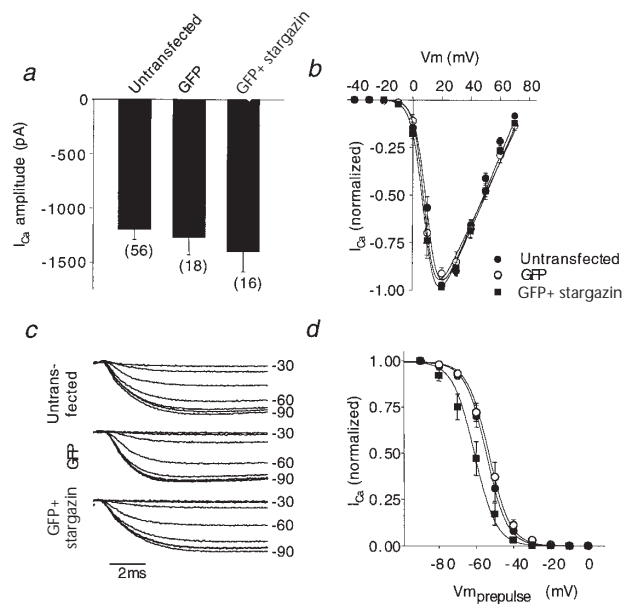


Fig. 6 Functional effect of stargazin on neuronal Ca^{2+} channel activity. **a**, Average whole-cell Ca^{2+} current in BHK cells. Currents were elicited by 40-ms pulses from a holding potential of -90 mV to a test potential of $+20$ mV in untransfected and transiently transfected cells expressing GFP alone or in combination with stargazin. Each bar represents mean \pm s.e. peak Ca^{2+} -current amplitude, and the number of recorded cells is indicated in parentheses. **b**, Average normalized current-voltage relationship for control and transfected BHK cells. Cells were held at -90 mV, and 40-ms command steps to the indicated voltages (V_m) were given sequentially at 20-s intervals. Peak currents measured at each command step were normalized to the maximum current observed in each cell, averaged and plotted as a function of voltage. Smooth curves are Boltzmann functions of the type $I_{\text{Ca}} = [g(\text{TP}-E)]/[1+\exp(-(\text{TP}-V_{1/2})/s)]$, where g is the maximum normalized conductance; E , the reversal potential; $V_{1/2}$, the potential of half activation; and s , the range of potential for an e-fold change around $V_{1/2}$. For the fitted control curve, $g=0.02$; $E=76$ mV; $V_{1/2}=-10$ mV; and $s=4.1$ mV. For the curve in cells transiently expressing GFP alone, $g=0.02$, $E=78$ mV, $V_{1/2}=-8$ mV and $s=3.7$ mV; and for the curve in cells co-expressing GFP and the stargazin protein, $g=0.02$, $E=78$ mV, $V_{1/2}=-8$ mV and $s=4.1$ mV. Symbols represent mean \pm s.e. of 6–14 cells. **c**, Representative superimposed current traces illustrating voltage-dependent inactivation of the channels at steady state from single control and transfected BHK cells. Individual currents in each cell were evoked by a 40-ms duration voltage step to $+20$ mV from a 5-s inactivating prepulse (ranging the voltages shown at the right) prior to the test potential. To facilitate comparison of records, currents have been scaled to similar size and only the first 10 ms are displayed. **d**, Average steady-state inactivation curves for control and transfected BHK cells. Currents were obtained as in (c). Values were expressed as a fraction of the maximum amplitude seen in each cell, averaged and plotted as a function of voltage. Curves were fitted with a single Boltzmann equation of the form $I_{\text{Ca}} = 1/[1+\exp((\text{TP}-V_{1/2})/s)]$, where $V_{1/2}$ is the voltage for 50% inactivation and s is the slope factor. For control cells, $V_{1/2}=-54.7 \pm 1.6$ mV and $s=5.6 \pm 0.5$ mV; for cells expressing GFP, $V_{1/2}=-53.4 \pm 1.9$ mV and $s=5.7 \pm 0.2$ mV; and for cells expressing GFP and stargazin, $V_{1/2}=-61.0 \pm 2.8$ mV and $s=5.8 \pm 0.2$ mV. Symbols represent pooled data from 6–7 cells.

dependent Ca^{2+} channels in a similar manner. For this, we used a BHK cell line that stably expresses neuronal α_1 class A (P/Q-type) Ca^{2+} channels ($\alpha_{1A}/\beta_{1A}/\alpha_2/\delta$; ref. 33).

A series of voltage protocols was used to compare the behaviour of the channels expressed with and without coexpression of stargazin. First, peak Ca^{2+} current amplitude was examined in response to 40-ms pulses in untransfected and transfected cells at a test potential of $+20$ mV (Fig. 6a). Although a small difference in current amplitude was observed upon coexpression of stargazin (-1200 ± 91 pA for control versus -1401 ± 184 pA for stargazin), the effect was not statistically significant. Likewise, the properties of the current-voltage relation of the Ca^{2+} currents were very similar between groups (Fig. 6b).

Although coexpression of stargazin with neuronal α_1 class A Ca^{2+} channels left the peak current-voltage relationship un-

changed, it significantly altered the balance between channel availability and inactivation (Fig. 6c,d). We measured steady-state inactivation of the Ca^{2+} channels with and without stargazin using a wide range of 5 s inactivating prepulses. Traces (Fig. 6c) show representative records of membrane currents in control and transfected cells at potentials ranging successively from -90 mV through -30 mV before a 40-ms step depolarization to a test potential of $+20$ mV. The results show that current amplitude is decreased as the channels became increasingly inactivated. Notably, the presence of stargazin accentuated this inhibition, shifting the voltage-dependence of channel availability towards more negative potentials. When measurements from individual cells were normalized and averaged, the midpoint voltage ($V_{1/2}$) was more negative in cells transfected with stargazin than in control cells, creating a statistically significant hyperpolarizing shift of approximately 7 mV in the voltage-dependence of neuronal α_1 class A Ca^{2+} -channel availability in the hypothesized direction (Fig. 6d; $P=0.017$; one-tailed test). These effects cannot be attributed to the mere presence of foreign protein in the plasma membrane of transfected cells, as coexpression of an unrelated protein did not affect α_1 class A Ca^{2+} channel gating (data not shown).

Discussion

Here we describe a new gene encoding a 36-kD transmembrane protein whose expression is disrupted in two independent alleles of stargazer mice. Stargazin is encoded by four exons, with a very large intron 1 spanning at least two stargazer (*stg*) distal recombinants on the genetic map²⁵. The *stg* allele is associated with the insertion of an ETn retrotransposon into intron 2. Several other mouse mutations have been caused by ETn insertions^{34–37}. As predicted for stargazer, in mutants where the ETn resides in an intron in the same transcriptional direction as the disrupted gene, the result is premature transcriptional termination, presumably within the element's LTR. RNA expression analysis of the waggler allele shows analogous expression defects mapping to intron 1, implying that the mutation may be due to a similar mechanism. Nevertheless, as the transcriptional termination appears incomplete in both mutant alleles, the construction of a true null mutation may be of value in future experiments.

The predicted protein structure of stargazin is similar to that of the γ subunit of skeletal muscle voltage-gated Ca^{2+} channels—the only γ subunit described to date—although stargazin is 100 aa longer at the C terminus. Its mRNA is expressed throughout the brain, with highest levels in the cerebellum, olfactory bulb, thalamus and hippocampus, similar to that of the α_{1A} Ca^{2+} channel subunit¹¹, but expression was not detected in other tissues. As in the case with known neuronal Ca^{2+} -channel subunits, stargazin is enriched in synaptic plasma membranes^{20,38,39}. Finally, stargazer's seizure phenotype is qualitatively like that of tottering and lethargic mouse mutants, which harbour defective Ca^{2+} -channel subunits. Together, these observations suggest that stargazin may be a new γ subunit for neuronal Ca^{2+} channels. In a test of this hypothesis, we found that stargazin shifts the voltage-dependence of inactivation of α_{1A} (P/Q-type) Ca^{2+} channels in BHK cells by approximately 7 mV, significantly reducing channel availability at a neuronal resting potential of -70 mV. This effect is due to the stabilization of channel inactivation rather than a simple block or lack of channel expression, and presumably occurs by direct interaction with other channel subunits, although intermediary components in the expression system cannot be excluded. Moreover, the effect of stargazin on P/Q-type Ca^{2+} channels mimics that of the skeletal muscle γ subunit on L-type channels, where the key effect is also a negative shift in the midpoint voltage of the steady-state channel inactivation curve^{27,30}.

P/Q-type Ca^{2+} channels are localized at presynaptic terminals and are the major mediators of Ca^{2+} entry and neurotransmitter release. Assuming that the effect of stargazin on channel inactivation is applicable to nerve terminals, where P/Q-type Ca^{2+} channels are abundant³⁹, stargazin is expected to inhibit presynaptic Ca^{2+} entry. In null or hypomorphic stargazer mutant mice, therefore, one expects inappropriate entry of Ca^{2+} into the cell. This may activate one or more second messenger systems which could explain, in part, the origin of stargazer's seizure phenotype. It is relevant to note that in cortical pyramidal neurons of stargazer mutants, the activity of a caesium-sensitive inward-rectifying current (I_h) was previously observed to be 2–3-fold higher than in wild-type cells⁴⁰. I_h is a mixed-cation inward-rectifying current that is inactive until the membrane potential becomes sufficiently hyperpolarized following an action potential. It has recently been shown that Ca^{2+}_i mediates the upregulation of the I_h current, probably through the action of second messengers⁴¹. Normally, deactivation of these currents results in the termination and a time period of prevention of synchronized oscillations in thalamocortical cells. If, however, I_h current deactivation is not present, as observed for stargazer, thalamic neurons display abnormal synchronized network oscillations with slow periodicity that last for seconds or tens of seconds, which are characteristic of absence epileptic seizures. The upregulation of I_h in stargazer mice is a plausible mechanistic link between a primary effect of this mutation and the absence seizure phenotype.

Inappropriate Ca^{2+} entry may also account for the molecular abnormalities described in the stargazer cerebellum. The cerebellar granular layer in stargazer has a 70-fold reduction of brain-derived neurotrophic factor (BDNF) mRNA (ref. 42), which is not easily explained by a loss of known receptors; for example, BDNF receptor (*TrkB*) message levels were normal. Given our findings, it seems reasonable to speculate that this BDNF downregulation, which probably contributes to stargazer's cerebellar ataxia and impaired conditioned eye-blink response⁴³, also occurs as a consequence of inappropriate Ca^{2+} entry.

Tottering and lethargic mouse mutants have defects in the α_{1A} and β_4 subunits of voltage-gated Ca^{2+} channels, and these mice have moderate cerebellar ataxia and spike-wave seizures similar to each other, but less pronounced than in stargazer^{44,45}. Contrary to those predicted for the stargazer mutant, the defects in the tottering mouse would anticipate reduced, not increased, Ca^{2+} entry into cells. Recent work shows that dissociated Purkinje cells from at least one allele of tottering have reduced P-type currents⁴⁶. Perhaps any perturbation in normal Ca^{2+} -channel activity can cause an imbalance in associated cellular mechanisms (for example, neurotransmitter release), resulting in spike-wave seizures; in stargazer, the additional downstream effect on I_h currents could account for its more pronounced spike-wave seizures. Alternatively, the anticipated phenotypic outcome for a mutant could be different if there are compensatory regulation of other channel subunits, as might be expected for the lethargic mutant given the similarities between β subunits¹². Furthermore, stargazin may have a unique interaction with a particular channel subunit, such as the recently cloned T-type channel, which is apparently not subject to β subunit regulation^{17,47}. Finally, it is tempting to speculate that while important for channel inactivation, stargazin has an additional 'downstream' function. For example, it may participate in direct protein signalling via its unique cytoplasmic C terminus; such a mechanism could be involved in the generation of spike-wave seizures. Clearly, there is still much to learn from the ion channel defects and the functional consequences of subunit interactions in these mouse mutants.

The discovery of stargazin, now known as the Ca^{2+} channel γ_2 subunit (*Cacng2*), completes the identification of all the major subunit types for neuronal Ca^{2+} channels, namely, α_1 , $\alpha_2\delta$, β and γ , although additional isoforms for a particular subunit type may exist. To gain further insight into γ_2 function, it will be important to define its influence on Ca^{2+} current diversity in neurons, for example, using functional assays with different neuronal α_1 genes, and to explore the major physical associations between *Cacng2* and other subunits. From these results, it will be possible to study channel function directly in mouse mutants in the most appropriate physiological and genetic contexts. This information will further our understanding of the native composition and function of voltage-gated Ca^{2+} channels so that they can be more effectively targeted in the treatment of neurological disorders.

Methods

Mice. The stargazer (*stg/stg*) and waggler (*stg^{wag}/stg^{wag}*) mice arose at The Jackson Laboratory as spontaneous mutations on A/J and MRL/MpJ inbred strains, respectively. Stargazer is now maintained on a hybrid C57BL/6J x C3HeB/FeJ background (B6C3Fe-*stg*) and waggler, on a C57BL/6J background (B6-*stg^{wag}*). All parental, control and mutant stocks are maintained at The Jackson Laboratory, where animal procedures were approved by ACUC.

Direct cDNA selection and library screening. Direct cDNA selection was performed with P1 and BAC clones as described²⁶ with modifications⁴⁸. The starting material for the preparation of cDNA selection products was poly(A) mRNA from adult A/J mouse brain. Total RNA was prepared using Trizol (GIBCO/BRL) and poly(A) mRNA was purified using oligo dT cellulose spin columns (Invitrogen). cDNA selection products had an average length of 500–600 bp. Of 400 cDNA selection products chosen for partial sequencing, about 30% from P12 had high similarity to intracisternal A-type particle proviruses, and about 10% from each clone were similar to moderately repetitive sequences. Twenty cDNA selection products clustered with an anonymous mouse brain EST mapped to chromosome 15 (MDB5079). A further twenty (derived from BAC28) were similar to an EST cluster later identified as the *Eif-3a66* gene, located on chromosome 22 (Unigene ID Hs.55682). Many cDNA selection products (Fig. 1a) were derived from incompletely spliced mRNA and contained intronic sequences. To find cDNA clones, the Lambda ZAP II ICR outbred mouse brain cDNA library (Stratagene) was screened with the ³²P-labelled cDNA selection product, c113, and phagemids were prepared from the positive plaques following the manufacturer's protocols. All radioactive probes were prepared using the Prime-It kit (Stratagene).

PCR and DNA sequencing. Mouse genomic DNA was prepared as described⁴⁹. DNA (5 $\mu\text{g}/\text{ml}$) was PCR amplified in a MJ Research PTC-100 machine (1 min 94 °C, 2 min 55 °C (62 °C for 3' end primer), 2 min 72 °C, for a total of 25–35 cycles). Primers were: 113F1 (5'–CTCAAAGCTTG-ATGACCATC–3'), 113R1 (5'–ACCATCTCGGCGATGATGAAG–3'), 113R2 (5'–ACGAAGAAGGTGCCAGCA–3'), Exon2OF (5'–TGCGGT-GTCAGCTTCGTAGTC–3'), 417-OR (5'–AAGTTCCCTTCGAGGCAG–3'), 109F (5'–CATTTCTGTCTCATCCTTTG–3'), EtN-OR (3' LTR) (5'–GCCTTGATCAGAGTAAGTGC–3'), JS167 (5' LTR) (5'–GAGCAAGCAGGTTTCAGGC–3') and E/Ht7 (5'–ACTGTCACTATCTGGAATC–3'). Intron regions, including intron/exon boundaries, and 5' and 3' ends were determined by subcloning fragments from P1 and BAC genomic DNA into pGEM1 vector (Promega). Following identification of the correct plasmids by colony hybridization⁵⁰, the inserts were subcloned into the pAMP10 vector (GIBCO/BRL) for automated sequencing. All genomic and cDNA clones were sequenced either manually with the Amplicycle sequencing kit (Perkin Elmer) or with the ABI model 373A automated DNA sequencer (Applied Systems) with M13 primers and the following primers. An overall 3–4-fold coverage of the complete ORF of the cDNA c2 and the 3' genomic region was determined. Internal primers were: C2R (5'–GCGGT-TATTGTTCTTGGCGGC–3'), C2F (5'–GGAAGTGTGGAACAGGAG-TCC–3'), 113OF (5'–TCTGGAGTACAGCCAATA–3'), C2F4 (5'–TGGAATTACCAATCGCACC–3'), 113OR (5'–TACGGCTGGTCTTC-TACTTC–3'), 113F2 (5'–TAGTAATATCATCGGGAT–3') and 3' end (5'–CCACGGGAAGACCTTCATA–3').

Northern blots and RT-PCR. Total RNA was prepared from adult mouse brains and 20 µg per lane was run on a 1.2% agarose/formaldehyde gel. Following blotting onto Nytran Plus membrane (Schleicher & Schuell), the blot was probed in formamide/hybridization buffer at 42 °C. The final wash was 0.1×SSC, 0.1% SDS at 65 °C. A 1.8-kb mouse actin probe was labelled and used as a control for equal RNA loading. RNA (5 µg) was reverse transcribed with AMV reverse transcriptase (Promega). PCR reactions were run as described above for 25 cycles. The control *B2m* primers were: F (5′-CACGCCACCCACCGGAGAATG-3′) and R (5′-GATGCTGATCACATGTCTCG-3′).

RNA *in situ* hybridization. C57BL/6J mice were perfused with 4% paraformaldehyde in PBS. Brains were collected and immersion-fixed for 12 h in 4% PFA/PBS at 4 °C followed by paraffin embedding. Sections (6 µm) were cleared in xylene, rehydrated in five graded ethanol steps, fixed with 4% PFA for 20 min, treated with proteinase K (20 µg/ml) for 7 min, refixed for 5 min, acetylated in 0.1 M triethanolamine/0.25% acetic anhydride for 10 min, dehydrated and air dried. The slides were hybridized with probe in hybridization mix (100 µl; 50% formamide, 1× Denhardt's, 10% dextran sulphate, 0.5 µg/ml yeast tRNA, 0.3 M NaCl, 5 mM EDTA, 10 mM Tris pH 8.0, 10 mM NaH₂PO₄ pH 6.8 and 5×10⁵ cpm/µl ³³P-labelled probe) for 16 h at 65 °C in a humid sealed chamber. Sense and antisense cRNA probes were transcribed from a 820-bp *EcoRI/PstI* DNA fragment containing the complete coding region of *Cacng2* with T3 or T7 polymerase (Promega) and [³³P]-UTP (NEN). Slides were washed twice in 5× SSC at 55 °C, 2×SSC/50% formamide at 65 °C for 30 min, rinsed, then RNase A treated for 15 min, washed again in 2×SSC/50% formamide at 65 °C for 30 min followed by a 2×SSC, 0.5×SSC wash, dehydrated in five graded ethanol steps and air dried. Exposures were overnight on Kodak Biomax MR film.

Construction and purification of maltose-binding protein (MBP)-stargazer fusion protein. Nucleotides 658–972 of the c2 clone ORF (aa 220–323) were amplified by PCR using the forward primer, 5′-TCTGAATTCGCCATCCGCCATCACCCGCATCCCCAGCTAC and the reverse primer, 5′-TATTTCTGCTGACTCTTTCATACTGGCGGTGGTCCGGCGGTTGG. The 350-bp product was ligated into *Sall/EcoRI* sites of pMal-c2 (New England Biolabs). The accuracy was confirmed by sequencing in both directions.

BL21(DE3) *E. coli*, transformed with pMal-*stg*, were induced (0.4 mM IPTG) for 3 h, then protease inhibitors (0.1 mM PMSF, 1 mM benzamide, 10 µg/ml leupeptin and aprotinin and 2 µg/ml pepstatin A) were added and the cells were collected by centrifugation at 4000g for 20 min. The cells were resuspended in buffer 1 (50 ml; 20 mM Tris-Cl, pH 7.4, 200 mM NaCl, 1 mM EDTA, 5 mM DTT, protease inhibitors), subjected to freeze/thaw, sonicated and centrifuged at 9000g for 30 min. The supernatant was diluted threefold with buffer 1 and rotated with amylose resin (3 ml; New England Biolabs) for 2 h at 4 °C. The column was washed with buffer 1 (30 ml) and eluted with buffer 1 that contained maltose (10 mM).

Development of stargazin antibody. A synthetic peptide (Research Genetics; CAA plus stargazer sequence DSLHANTANRRRTTPV) was coupled to keyhole limpet hemocyanin (KLH) for injection into rabbit 239 (ref. 51). Serum was affinity-purified⁵² against MBP-stargazin fusion protein.

Gel electrophoresis and western-blot analysis. Mouse 2× KCl-washed brain microsomes and synaptic plasma membranes were prepared as described^{53,54}. Reduced, denatured samples were applied to SDS-polyacrylamide gels⁵⁵. Gels were stained with Gelcode Coomassie blue reagent (Pierce) or transferred to Immobilon NC (Millipore) in transfer buffer that contained 20% methanol (40 V, 6 h, 4 °C).

All blotting steps were carried out in 5% non-fat dry milk in PBS (pH 7.4; ref 51). The blot was incubated with primary antibody (1:100) for 12 h at 4 °C and with HRP-conjugated goat anti-rabbit antibody (1:20,000; Boehringer Mannheim) for 1 h at RT. Detection was made with SuperSignal ECL reagent (Pierce) and Kodak X-OMAT film.

Immunoprecipitation of [³⁵S]-Met-labelled stargazin. Radiolabelled stargazin was prepared as instructed in the *in vitro* coupled transcription/translation rabbit reticulocyte lysate system kit (Promega) using T7 RNA polymerase, 40 µCi of [³⁵S]-Met (Amersham; 10 mCi/ml) and 0.6 µg of pcDNA3-*stg* in 50 µl reaction volume. Unincorporated [³⁵S]-Met was

removed by centrifugal gel filtration and the reaction mix was eluted in a total volume of 1400 µl. Antibody beads were prepared by incubating a 1:1 ratio of either rabbit preimmune serum or antibody 239 with Protein G-Sepharose (Pharmacia) overnight at 4 °C, followed by 3 washes in PBS. Antibody beads (30 µl) were rotated for 4 h at 4 °C with 300 µl of [³⁵S]-stargazin. Beads were collected by centrifugation, washed three times with column buffer and bound material eluted with gel loading buffer. Following SDS-PAGE, the gel was washed, dried and exposed to Kodak BioMax MR film.

Cell culture and transfection. The cell line BHKBI-6 stably expressing the α_{1A} , $\alpha_{2\delta}$ and β_{1A} subunits was established by transfection of baby hamster kidney (BHK) cells with the plasmids pK4KBI (α_{1A}), pCAA2 ($\alpha_{2\delta}$) and pCABE (β_{1A}) and selection in Dulbecco's modified Eagle's medium (DMEM) containing G418 and methotrexate³³. The cells were grown in supplemented DMEM (5% fetal bovine serum, 30 U/ml penicillin, 30 µg/ml streptomycin, 250 µM methotrexate and 600 µg/ml G418) at 37 °C in a 5% CO₂ humidified atmosphere. Cells were fed every other day and subcultured once weekly up to passage eight. Transient transfections were performed using the calcium-phosphate method⁵⁶ with 3 µg of plasmid cDNA encoding the mouse stargazin protein. The construct was made by assembling a *HindIII/KpnI* 1.5-kb fragment of the c2 clone containing the entire ORF into the pcDNA3 expression vector (Invitrogen). To select positively transfected cells for electrophysiology, a plasmid encoding the green fluorescent protein (pGreen Lantern-1; GIBCO/BRL) was added to the DNA transfection mixture (1:1).

Current recordings. Ca²⁺-channel currents were recorded from BHK cells according to the whole-cell patch-clamp technique⁵⁷. All recordings were performed at RT using an Axopatch 200A patch-clamp amplifier (Axon Instruments) and 2–4 M Ω micropipettes manufactured from borosilicate glass capillary tubes. Cells were clamped at a holding potential of –90 mV and capacity transients were electronically compensated. Currents were evoked by 40-ms depolarizing voltage steps (0.05 Hz) to test potentials ranging from –40 to +70 mV. To measure Ca²⁺-channel inactivation at steady-state, cells were held for 5 s at potentials ranging successively from –90 through 0 mV prior to a 40-ms step depolarization to a test potential of +20 mV. Linear leak and residual capacity currents were subtracted on-line using a P/4 standard protocol. Current records were captured on-line and digitized at a sampling rate of 20 kHz following filtering of the current record (5 kHz; 4-pole Bessel filter) using a personal computer attached to a TL-1 interface (Axon). Pulse protocols, data capture and analysis of recordings were performed using pCLAMP software (Axon). To isolate Ca²⁺ currents, cells were bathed in a solution containing (in mM): CaCl₂ 10, tetraethylammonium chloride (TEA-Cl) 125, HEPES 10, glucose 5. The bath solution was adjusted to pH 7.3 with TEA-OH and to 300 mosm l⁻¹ with sucrose. The internal (patch pipette) solution consisted of (mM): CsCl 135, MgCl₂ 5, EGTA 10, HEPES 10, ATP (magnesium salt) 4, GTP 0.1 (pH 7.3/CsOH, 286 mosm l⁻¹). The statistical significance of differences in mean current amplitude and V_{1/2} between cells expressing stargazer and control was determined by one-way ANOVA, followed by Duncan's new multiple range test.

GenBank accession numbers. *Cacng2*, AF077739; rat Ca²⁺-channel γ subunit, EMBL Y09453.

Acknowledgements

We thank P. Nishina for the cDNA library, S. Ackerman, S. Przyborski, J. Gervais, S. Hipkens, A. Costa, G. Yellen, K. Shin, L. Salkoff and R. Coral for advice or assistance at various points in the project and C. Dunbar for expert animal care. We are also grateful to G. Cox and S. Ackerman for review of a preliminary version of this manuscript, and The Jackson Laboratory Mouse Mutant Resource for providing mice. This work was supported by NIH grant NS32801 to V.A.L. and a Klingenstein Fellowship in the Neurosciences to W.N.F. R.F. is supported by a Human Frontier Science Program postdoctoral fellowship. K.P.C. is an investigator of the Howard Hughes Medical Institute. G.H.B. is supported in part by a fellowship from the U. of Iowa Cardiovascular Center.

Received 15 June; accepted 10 July, 1998.

1. Ottman, R., Hauser, W.A., Barker-Cummings, C., Lee, J.H. & Risch, N. Segregation analysis of cryptogenic epilepsy and an empirical test of the validity of the results. *Am. J. Hum. Genet.* **60**, 667–675 (1997).
2. Charlier, C. *et al.* A pore mutation in a novel KQT-like potassium channel gene in an idiopathic epilepsy family. *Nature Genet.* **18**, 53–55 (1998).
3. Singh, N.A. *et al.* A novel potassium channel gene, KCNQ2, is mutated in an inherited epilepsy of newborns. *Nature Genet.* **18**, 25–29 (1998).
4. Biervert, C. *et al.* A potassium channel mutation in neonatal human epilepsy. *Science* **279**, 403–406 (1998).
5. Smart, S.L. *et al.* Deletion of the Kv1.1 potassium channel causes epilepsy in mice. *Neuron* **20**, 809–819 (1998).
6. Homanics, G.E. *et al.* Mice devoid of gamma-aminobutyrate type A receptor beta3 subunit have epilepsy, cleft palate, and hypersensitive behavior. *Proc. Natl Acad. Sci. USA* **94**, 4143–4148 (1997).
7. Brusa, R. *et al.* Early-onset epilepsy and postnatal lethality associated with an editing-deficient GluR-B allele in mice. *Science* **270**, 1677–1680 (1995).
8. Noebels, J.L. Mutational analysis of inherited epilepsies. In *Basic Mechanisms of the Epilepsies: Molecular and Cellular Approaches*. (eds Delgado-Escueta, A.V., Ward, A.A., Woodbury, D.M. & Porter, R.J.) **44**, 97–113 (Raven Press, New York, 1986).
9. Noebels, J.L., Qiao, X., Bronson, R.T., Spencer, C. & Davisson, M.T. Stargazer: a new neurological mutant on Chromosome 15 in the mouse with prolonged cortical seizures. *Epilepsy Res.* **7**, 129–135 (1990).
10. Cox, G.A. *et al.* Sodium/hydrogen exchanger gene defect in slow-wave epilepsy mutant mice. *Cell* **91**, 1–20 (1997).
11. Fletcher, C.F. *et al.* Absence epilepsy in tottering mutant mice is associated with calcium channel defects. *Cell* **87**, 607–617 (1996).
12. Burgess, D.L., Jones, J.M., Meisler, M.H. & Noebels, J.L. Mutation of the Ca²⁺ channel β subunit gene *Cchb4* is associated with ataxia and seizures in the lethargic (*lh*) mouse. *Cell* **88**, 385–392 (1997).
13. Bito, H., Deisseroth, K. & Tsien, R.W. Ca²⁺-dependent regulation in neuronal gene expression. *Curr. Opin. Neurobiol.* **7**, 419–429 (1997).
14. Dunlap, K., Leubke, J.I. & Turner, T.J. Exocytotic calcium channels in mammalian central neurons. *Trends Neurosci.* **18**, 89–98 (1995).
15. Varadi, G., Mori, Y., Mikala, G. & Schwartz, A. Molecular determinants of Ca²⁺ channel function and drug action. *Trends Pharmacol. Sci.* **16**, 43–49 (1995).
16. Nooney, J.M., Lambert, R.C. & Feltz, A. Identifying neuronal non-L Ca²⁺ channels — more than stamp collecting? *Trends Pharmacol. Sci.* **18**, 363–371 (1997).
17. Perez-Reyes, E. *et al.* Molecular characterization of a neuronal low-voltage-activated T-type calcium channel. *Nature* **391**, 896–900 (1998).
18. De Waard, M., Gurnett, C.A. & Campbell, K.P. Structural and functional diversity of voltage-activated calcium channels. In *Ion Channels* (ed. Narahashi, T.) 41–87 (Plenum Press, New York, 1996).
19. Jay, S.D. *et al.* Primary structure of the γ subunit of the DHP-sensitive calcium channel from skeletal muscle. *Science* **248**, 490–492 (1990).
20. Ludwig, A., Flockerkzi, V. & Hofmann, F. Regional expression and cellular localization of the $\alpha 1$ and β subunit of high voltage-activated calcium channels in rat brain. *J. Neurosci.* **17**, 1339–1349 (1997).
21. Walker, D. & De Waard, M. Subunit interaction sites in voltage-dependent Ca²⁺ channels: role in channel function. *Trends Neurosci.* **21**, 148–154 (1998).
22. Scott, V.E.S. *et al.* β subunit heterogeneity in N-type Ca²⁺ channels. *J. Biol. Chem.* **271**, 3207–3212 (1996).
23. Liu, H. *et al.* Identification of three subunits of the high affinity ω -conotoxin MVIIC-sensitive Ca²⁺ channel. *J. Biol. Chem.* **271**, 13804–13810 (1996).
24. Sweet, H.O., Bronson, R.T., Cook, S., Spencer, C. & Davisson, M.T. Research News. 1. Wagglers (*wag*). *Mouse Genome* **89**, 552 (1991).
25. Letts, V.A. *et al.* Genetic and physical maps of the stargazer locus on mouse Chromosome 15. *Genomics* **43**, 62–68 (1997).
26. Morgan, J.G., Dolganov, G.M., Robbins, S.E., Hinton, L.M. & Lovett, M. The selective isolation of novel cDNAs encoded by the regions surrounding the mouse interleukin 4 and 5 genes. *Nucleic Acids Res.* **20**, 5173–5179 (1992).
27. Eberst, R., Dai, S., Klugbauer, N. & Hofmann, F. Identification and functional characterization of a calcium channel γ subunit. *Pflügers Arch. - Eur. J. Physiol.* **433**, 633–637 (1997).
28. Wissenbach, U. *et al.* The structure of the murine calcium channel γ -subunit gene and protein. *Biol. Chem.* **379**, 45–50 (1998).
29. Scott, V.E.S., Felix, R., Arikath, J. & Campbell, K.P. Evidence for a 95 kDa short form of the $\alpha 1A$ subunit associated with the ω -Conotoxin MVIIC receptor of the P/Q-type Ca²⁺ channels. *J. Neurosci.* **18**, 641–647 (1998).
30. Singer, D. *et al.* The roles of the subunits in the function of the calcium channel. *Science* **253**, 1553–1557 (1991).
31. Wei, X.Y. *et al.* Heterologous regulation of the cardiac Ca²⁺ channel $\alpha 1$ subunit by skeletal muscle β and γ subunits. Implications for the structure of cardiac L-type Ca²⁺ channels. *J. Biol. Chem.* **266**, 21943–21947 (1991).
32. Lerche, H., Klugbauer, N., Lehmann-Horn, F., Hofmann, F. & Melzer, W. Expression and functional characterization of the cardiac L-type calcium channel carrying a skeletal muscle DHP-receptor mutation causing hypokalaemic periodic paralysis. *Pflügers Arch. - Eur. J. Physiol.* **431**, 461–463 (1996).
33. Niidome, T. *et al.* Stable expression of the neuronal BI (class A) calcium channel in baby hamster kidney cells. *Biochem. Biophys. Res. Commun.* **203**, 1821–1827 (1994).
34. Steinmeyer, K. *et al.* Inactivation of muscle chloride channel by transposon insertion in myotonic mice. *Nature* **354**, 304–308 (1991).
35. Adachi, M., Watanabe-Fukunaga, R. & Nagata, S. Aberrant transcription caused by the insertion of an early transposable element in an intron of the Fas antigen gene of *Ipr* mice. *Proc. Natl Acad. Sci. USA* **90**, 1756–1760 (1993).
36. Herrmann, B.G. & Kispert, A. The *T* genes in embryogenesis. *Trends in Genet.* **10**, 280–286 (1994).
37. Moon, B.C. & Friedman, J.M. The molecular basis of the obese mutation in *ob2j* mice. *Genomics* **42**, 152–156 (1997).
38. Leveque, C. *et al.* Purification of the N-type calcium channel associated with syntaxin and synaptotagmin. A complex implicated in synaptic vesicle exocytosis. *J. Biol. Chem.* **271**, 13804–13810 (1994).
39. Westenbroek, R.E. *et al.* Immunohistochemical identification and subcellular distribution of the $\alpha 1A$ subunits of brain calcium channels. *J. Neurosci.* **15**, 6403–6418 (1995).
40. Di Pasquale, E., Keegan, K.D. & Noebels, J.L. Increased excitability and inward rectification in layer V cortical pyramidal neurons in the epileptic mutant mouse Stargazer. *J. Neurophysiol.* **77**, 621–631 (1997).
41. Lüthi, A. & McCormick, D.A. Periodicity of thalamic synchronized oscillations: the role of Ca²⁺-mediated upregulation of Ih. *Neuron* **20**, 553–563 (1998).
42. Qiao, X., Heftli, F., Knusel, B. & Noebels, J.L. Selective failure of brain-derived neurotrophic factor mRNA expression in the cerebellum of stargazer, a mutant mouse with ataxia. *J. Neurosci.* **16**, 640–648 (1996).
43. Qiao, X. *et al.* Selective failure of TDNF/TrkB signal transduction in cerebellum associated with impairment of classical eyeblink conditioning in stargazer mutant mice. *J. Neurosci.* in press, (1998).
44. Noebels, J.L. & Sidman, R.L. Inherited epilepsy: Spike-wave and focal motor seizures in the mutant mouse tottering. *Science* **204**, 1334–1336 (1979).
45. Hosford, D.A. *et al.* The role of GABAB receptor activation in absence seizures of lethargic (*lh/lh*) mice. *Science* **257**, 398–401 (1992).
46. Lorenzon, N.M., Lutz, C.M., Frankel, W.N. & Beam, K.G. Altered calcium channel currents in Purkinje cells of the neurological mutant mouse leaner. *J. Neurosci.* **18**, 4482–4489 (1998).
47. Lambert, R.C. *et al.* T-type Ca²⁺ current properties are not modified by Ca²⁺ channel β subunit depletion in nodosus ganglion neurons. *J. Neurosci.* **17**, 6621–6628 (1997).
48. Segre, J.A., Nemhauser, J.L., Taylor, B.A., Nadeau, J.H. & Lander, E.S. Positional cloning of the nude locus: genetic, physical, and transcription maps of the region and mutations in the mouse and rat. *Genomics* **28**, 549–559 (1995).
49. Taylor, B.A., Rowe, L. & Grieco, D.A. The MEV mouse linkage testing stock: mapping 30 novel proviral insertions and establishment of an improved stock. *Genomics* **16**, 380–394 (1993).
50. Sambrook, J., Fritsch, E.F. & Maniatis, T. *Molecular Cloning: A Laboratory Manual 2nd Edition*. (Cold Spring Harbor Laboratory Press, Cold Spring Harbor, New York, 1989).
51. Harlow, E. & Lane, D. *Antibodies, A Laboratory Manual*. (Cold Spring Harbor Laboratory Press, Cold Spring Harbor, New York, 1988).
52. Sharp, A.H. & Campbell, K.P. Characterization of the 1,4-dihydropyridine receptor using subunit-specific polyclonal antibodies. Evidence for a 32,000-Da subunit. *J. Biol. Chem.* **264**, 2816–2825 (1989).
53. Jones, D.H. & Matus, A.I. Isolation of synaptic plasma membrane from brain by combined flotation-sedimentation density gradient centrifugation. *Biochim. Biophys. Acta* **356**, 276–287 (1974).
54. Witcher, D.R., De Waard, M., Kahl, S.D. & Campbell, K.P. Purification and reconstitution of N-type calcium channel complex from rabbit brain. *Meth. Enzymol.* **238**, 335–348 (1994).
55. Laemmli, U.K. Cleavage of structural proteins during the assembly of the head of bacteriophage T4. *Nature* **227**, 680–685 (1970).
56. Kingston, R.E. Introduction of DNA into mammalian cells. In *Current Protocols in Molecular Biology*, (eds Ausubel, F.M. *et al.*) 9.1.1–9.1.11 (John Wiley & Sons, New York, 1997).
57. Hamill, O.P., Marty, A., Neher, E., Sakmann, B. & Sigworth, F.J. Improved patch-clamp techniques for high resolution current recording from cells and cell-free membrane patches. *Pflügers Arch. - Eur. J. Physiol.* **391**, 85–100 (1981).
58. Altschul, S.F. *et al.* Gapped BLAST and PSI-BLAST: a new generation of protein database search programs. *Nucleic Acids Res.* **25**, 3389–3402 (1997).
59. Hofmann, K. & Stoffel, W. TMbase - A database of membrane spanning proteins segments. *Biol. Chem. Hoppe-Seyler* **347**, 166 (1993).